ADVANCED FUNCTIONAL MATERIALS
www.afm-journal.de

Polysiloxane Inks for Multimaterial 3d Printing of High-Permittivity Dielectric Elastomers

Patrick M. Danner, Tazio Pleij, Gilberto Siqueira, Alexandra V. Bayles, Thulasinath Raman Venkatesan, Jan Vermant, and Dorina M. Opris**

Dielectric elastomer transducers (DET) are promising candidates for electrically-driven soft robotics. However, the high viscosity and low yield stress of DET formulations prohibit 3D printing, the most common manufacturing method for designer soft actuators. DET inks optimized for direct ink writing (DIW) produce elastomers with high stiffness and mechanical losses, diminishing the utility of DET actuators. To address the antagonistic nature of processing and performance constraints, principles of capillary suspensions are used to engineer DIW DET inks. By blending two immiscible polysiloxane liquids with a filler, a capillary ink suspension is obtained, in which the ink rheology can be tuned independently of the elastomer electromechanical properties. Rheometry is performed to measure and optimize processibility as a function of filler and secondary liquid fraction. Including polar polysiloxanes as the secondary liquid produces a printed elastomer exhibiting a four-fold permittivity increase over commercial polydimethylsiloxane. The characterization and multimaterial printing into layered DET devices demonstrates that the immiscible capillary suspension improves the processability of the inks and enhances the properties of the elastomers, enabling actuation of the devices at comparatively low voltages. It is anticipated that this formulation approach will allow soft robotics to harness the full potential of DETs.

1. Introduction

Recent advances in 3D printing have expanded the materials, types, sizes, and shapes of soft actuators. Magnetic, pneumatic, pH, and light-induced actuators have been successfully printed in various configurations by extrusion-based processes, such as direct ink writing (DIW).[1–5] Yet, despite intense research, successful examples of printed electrically-driven dielectric elastomer actuators (DEA) remain rare.[6,7] While hydraulically amplified actuators can be 3D printed by inkjet printing, the ink requirements imposed by DIW create a significant challenge for DEA.[8] So far, DIW DEA have been manufactured by printing the electrode ink and filling in the dielectric liquid in a post-processing step or by co-extrusion of core-shell or helical fibers.[9–11] While these examples are promising, the design freedom is significantly restricted. In the former, structures that allow for post-filling are required, and in the latter, the capacitor layout is fixed to fiber structures. Additionally, voltages of up to 10 kV are needed to achieve significant actuation. One reason for the few examples of direct ink-writing DEAs is the mismatch in processing and elastomer rheological requirements. Additionally, the dielectric layers in DEAs must be thin (< 100 µm) and uniform for reliable operation, whereas DIW structures tend to have rough surfaces with relatively large line thicknesses (100 µm up to few mm). The high thickness and the low dielectric permittivity of dielectric elastomer films necessitates high driving voltages for actuation. Additionally, the trade-offs between ink requirements for processing and cross-linked elastomer

P. M. Danner, T. R. Venkatesan, D. M. Opris
Laboratory for Functional Polymers
Swiss Federal Laboratories for Materials Science and Technology – Empa
Ueberlandstr. 129, Dübendorf CH-8600, Switzerland
E-mail: dorina.opris@empa.ch

P. M. Danner, T. Pleij, G. Siqueira, A. V. Bayles, J. Vermant, D. M. Opris
Departments of Materials
ETH Zürich
Vladimir-Prelog-Weg 5, Zürich CH-8093, Switzerland
E-mail: jan.vermant@mat.ethz.ch

G. Siqueira
Cellulose and Wood Materials Laboratory
Swiss Federal Laboratories for Materials Science and Technology – Empa
Ueberlandstr. 129, Dübendorf CH-8600, Switzerland

A. V. Bayles
Department of Chemical and Biomolecular Engineering
University of Delaware
Newark, Delaware 19716, USA

The ORCID identification number(s) for the author(s) of this article can be found under https://doi.org/10.1002/adfm.202313167

DOI: 10.1002/adfm.202313167

parameters impact the device actuation performance. Therefore, novel inks are required to enable fully DIW-printed DEA with performance comparable to conventionally manufactured devices.

One solution is to increase the dielectric permittivity of the dielectric film. Strategies that increase the permittivity of elastomers and subsequently decrease the driving voltage include incorporating ceramic fillers, conductive fillers, ionic liquids, or chemical modification with polar groups into the DEA formulation.[12–16] Chemical modification of polysiloxanes with different polar groups has resulted in high-permittivity polysiloxanes with excellent actuation.[17–20] Silicones modified with cyano groups have been shown to have among the highest permittivity of ≈18 and excellent actuator performance.[16,20,21] In principle, these high-permittivity elastomers could compensate for the thick structures created by direct ink-writing and produce elastomers that actuate at practical driving voltages. However, high-permittivity elastomers have only been processed by traditional thin-film methods such as blade casting or slot-die coating, which require solvents for processing.[15,18–20,22] Additionally, only a few multi-layered structures consisting of three active layers have been reported for polar polysiloxanes (PP), demonstrating the additional processing challenges this new class of materials faces even on well-established thin-film techniques.[19,21,23–26]

As with polar polysiloxane inks, conventional polydimethylsiloxane (PDMS) inks require significant modification to be processable by DIW. Reliable extrusion requires that DIW inks meet certain rheological criteria. Generally, ink formulations must exhibit a high degree of shear thinning, G' higher than a few kPa, G' exceeding G'' in the linear viscoelastic regime, recovery of viscosity within seconds after exiting the nozzle and yield stress at rest on the order of few 100 Pa.[7,27,28] While these benchmarks are used throughout 3D printing literature and are helpful for practitioners to find the right ink formulation window, it should be noted that all values are rough guidelines. In fact, some of these metrics encompass similar and dependent information, such as the elastic response, which is here defined by both G' and the yield stress separately. DIW printability of PDMS-based inks is generally achieved through dense packing of stiff inorganic fillers, such as fumed silica. Percolated filler networks exhibit sufficient shear thinning and yield stress and subsequently print with high fidelity.[28] However, high filler fractions in ink produce elastomers with relatively high stiffness (>1 MPa) and mechanical losses ($\tan(\delta) > 0.1$).[10,29] In contrast, elastomers formulated for DEA applications and generally processed by thin film techniques are soft (<1 MPa), possess low mechanical losses with $\tan(\delta) < 0.1$ and low Mullins and Payne effects, while retaining high permittivity.[19,25] Decreasing Young's modulus of DIW printed structures containing a high amount of fillers can thus only be achieved through partial cross-linking of the matrix, which increases mechanical losses. This trade-off was described in-depth by Chortos et al., who carefully tuned the composition to reach DIW printable inks with acceptable Young's moduli of 750 kPa of the cross-linked elastomer, however, the mechanical losses are still rather high with a $\tan(\delta)$ of 0.155.[10] To achieve soft (< 1 MPa) elastomers with good elasticity ($\tan(\delta) \leq 0.05$), not only the filler fraction should be low, but the molar mass between cross-links should be large. This requires high molar mass polymers, which are difficult to process due to their high viscosity and resulting pressure requirements during extrusion. Thus, the ink and final elastomer properties are interlinked and cannot be separated, leading to unfavorable trade-offs between ink rheology and elastomer electromechanical properties.[9]

To address these trade-offs in PDMS-based inks, different strategies have been applied, such as printing into support baths, adding wax particles, thiols, PEG, glycerol, cross-linked PDMS microspheres instead of inorganic fillers, commercial thixotropic additives, or complex custom-made additives.[3,29–35] However, thus far, none of these strategies has been employed for DIW of DETs. While some of these strategies might work for DET applications, liquid additives and solvents are often attributed to negatively affecting the electrical breakdown field or to increase aging effects, such as the leaking of liquids from the cross-linked elastomer.[15,35,36] Additives that are removed from the cross-linked elastomer after processing, such as wax particles, ultimately create porous structures, which are also not suitable for DEA applications due to the low dielectric breakdown strength of air (≈3 $V\mu m^{-1}$). Besides removing a solid additive (e.g., wax), liquid additives are sometimes removed from the printed structure. This is often the case in capillary suspension inks.

Capillary suspensions allow manipulation of ink rheology independently of specific elastomer chemistry, which dictates the final elastomer properties.[36] Instead of using dense filler packings to generate network structures, a secondary immiscible fluid is added to the primary fluid-particle dispersion to create capillary bridges in either a pendular or a capillary state. The bridges can generate strong gels that can be readily printed. This approach has been explored before for DIW printing of PDMS, however, the secondary immiscible fluid was removed in a post-processing step, leading to the previously mentioned detrimental performance if it were applied to DET applications.[37–40] Notably, immiscible polysiloxane-water suspensions with cross-linked PDMS microbeads as filler have been DIW printed.[1,32] The water removal after cross-linking created porous elastomers with a dielectric breakdown field that is too low for DEA applications. Thus, developing a capillary suspension, where the primary and secondary liquid remain in the cross-linked elastomer, would help achieve 3D printable, low-filler, continuous composites.

Here, we formulate a two-phase capillary suspension using polar and non-polar polysiloxane. In contrast to previously reported capillary suspension inks, both fluids remain in the network after printing and cross-linking, leading to non-porous, solid elastomers. The polar polysiloxane (PP) additive brings several functionalities simultaneously: it improves ink printability while increasing the elastomer's permittivity and elasticity and while decreasing Young's modulus and Payne and Mullins effects. The synergistic improvements of printability and electromechanical properties lead to 3D printable DET with improved device performance, significantly reducing the operating electric field. This novel dielectric ink, combined with multimaterial printing of dielectric and electrode, opens new and simple routes to realize complex 3D structures of electrically actuated soft robots. In the following, we describe how to systematically formulate the ink by optimizing the rheology for DIW and then optimizing the electromechanical properties to ultimately achieve functional DEA devices.

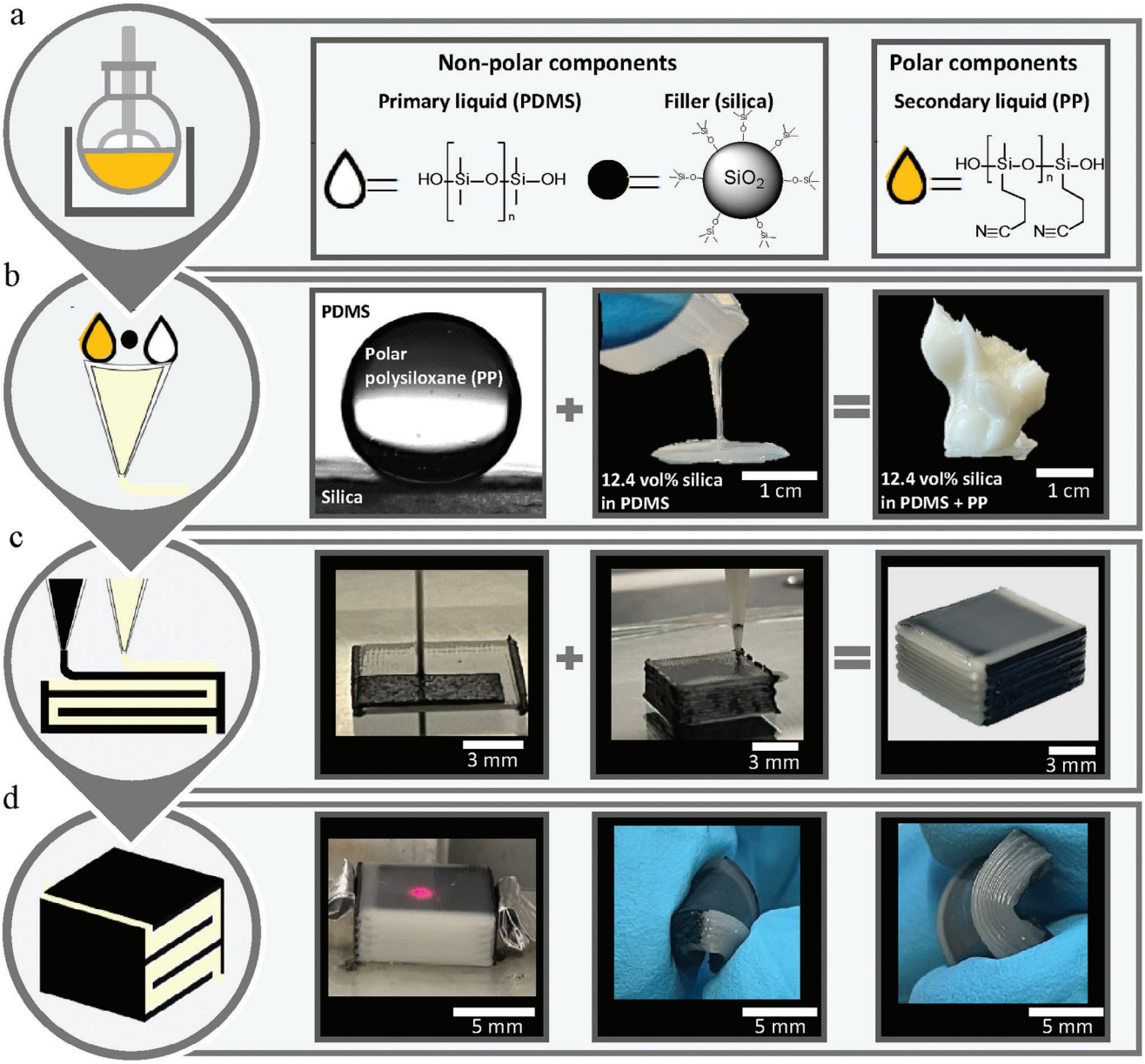

Figure 1. Overview of the process from synthesis to 3D printed stack dielectric elastomer actuators. a) Polymer synthesis starting from PP, non-polar silanol-terminated PDMS, and hydrophobic fumed silica. b) Ink preparation to achieve DIW printable capillary suspension. From left to right: Three-phase contact angle measurement, a droplet of PP in PDMS on a hydrophobic fumed silica surface. Flowing and spreading of a PDMS containing 12.4 vol% fumed silica. DIW printable ink with 12.4 vol% fumed silica, PDMS, and 30 vol% PP. c) Multimaterial printing of a conductive ink and high-permittivity capillary suspension ink to create a stack DET. From left to right: Printing the first interdigitated electrode ink and the last dielectric ink layer. Finished printed but uncross-linked 23 layers stack dielectric elastomer actuator with dielectric and electrode thicknesses of 200 and 120 µm, respectively. d) Final printed and cross-linked soft and deformable elastomer actuator connected to Al wires as well as its compress and stretchability.

2. Results and Discussion

2.1. Ink Based on Polar and Non-Polar Polysiloxane Suspension

Preparing a DIW-printed, stack DET involved synthesizing high-permittivity polar polysiloxane fluids, optimization of the dielectric and conductive inks to meet the rheological properties required for multimaterial printing as well as adjusting elastomer electromechanical properties after cross-linking, and finally, use the developed inks to manufacture stack DET (**Figure 1**). The selection of the ink components and their composition is crucial for reconciling printability with the electromechanical elastomer properties. The primary liquid of the capillary suspension is a silanol-terminated PDMS of low molecular weight of 2–3.5 kg·mol^{-1}, or an average of 27–47 repeat units per chain (Figure 1a). The low molecular weight PDMS has a low kinematic viscosity (45–85 cSt), which facilitates processing, as polysiloxane chains with a molecular weight of 12 kg mol^{-1} and above

entangle.[41] Chain entanglements lead to undesired pressure gradients during processing, the occurrence of elastic recoil, and the formation of threads at the nozzle due to increased elongational viscosity. Moreover, high-viscosity polymers require higher pressures during printing than low-viscosity ones at equal flow rates, which engenders practical challenges for pumps, tubing, or the possibility of nozzle failure, often limiting the minimum nozzle diameter. The better processing conditions of low-viscosity PDMS inks are combined with lower mechanical losses in the final elastomer, making it the logical choice, provided the ink stability after deposition is maintained.

The low molecular weight PDMS has fewer entanglements and inter-chain interactions, leading to the low viscosity of 44–82 mPa s, and hence would typically require large amounts of filler to achieve yield stresses in the order of few 100 Pa, sufficient for DIW. However, such high solids loading is detrimental to the final elastomer's electromechanical performance. We avoided high filler loading by creating a capillary suspension using a lower volume fraction of particles (as low as 6.3 vol%) and a second PDMS-immiscible fluid, polar cyanopropyl-modified polysiloxane (PP). The PP behaves like a Newtonian fluid, typical for polysiloxanes, with a viscosity of 6.65 ± 0.08 Pa s (Figure S1, Supporting Information, G″ consistently exceeds *G'* and the viscosity is constant for shear rates between 0.1–100 s^{-1}). The three-phase contact angle of the PP with silica in the presence of PDMS was as high as 150.3° (Figure 1b; Figure S2, Supporting Information). Three-phase contact angles between 90°–151.2° promote the formation of capillary suspensions, with smaller angles leading to wetting of the particles and larger angles leading to complete dewetting.[42,43] The difference in polarity between the two liquids causes phase separation of the two polysiloxanes even while subjected to heating or strong, prolonged mixing. The polarity difference can be described by the difference in dielectric permittivity, where the PDMS has a relative permittivity of 2.75 and the PP a relative permittivity of 18.16 ± 1.50 (at AC fields between $5{\cdot}10^5$–$5{\cdot}10^4$ Hz, Figure S3, Supporting Information), leading to a polarity difference of $\Delta\epsilon'$ of 15.41 ± 1.50.

An ink formulation consisting of 12.4 vol% fumed silica filler in the short chain PDMS flows and readily spreads on any substrate, as the volume fraction is below the percolation threshold. Such formulations are unsuitable for printing as they spread after extrusion due to insufficient yield stresses significantly below 100 Pa. The 12.4 vol% silica is approximately half the silica volume needed to achieve a printable ink by creating a percolated network through dense packing of the particles. Instead of dense packing, a capillary network is created by adding a small amount of the second immiscible liquid to the base formulation (in the order of a few vol%). After the PP is added as the third component, an ink with an appreciable yield stress is formed, as is qualitatively visible in Figure 1b. Thus, the three components (silica particles, PDMS, and PP) create printable inks with suitable rheological properties for DIW, as mentioned earlier, with a high degree of shear thinning, *G'* higher than a few kPa, *G'* exceeding *G″* in the linear viscoelastic regime, recovery of viscosity within seconds after exiting the nozzle and a yield stress at rest in the order of few 100 Pa.[7,27,28]

Two non-polar components are added to the ink to cross-link the printed structures into an elastomer. A (25%–35% methylhydrosiloxane-*co*-dimethylsiloxane) polymer serves as a PDMS-miscible cross-linker and has a low viscosity of 25–35 cSt. Lastly, the addition of dibutyltin dilaurate is needed as it catalyzes the condensation reaction. The suspension can then be printed directly using DIW into arbitrary structures such as hollow cones, hollow cubes, or multilayer grids. In combination with a printable electrode ink, multimaterial printing enables the facile creation of a stack DET consisting of alternating electrode and dielectric elastomer layers (Figure 1c). The cross-linked stack DET devices are stretchable, deformable, and soft and can subsequently function as tactile sensors or actuators (Figure 1d).

To quantify the impact of the secondary liquid on the ink composition, the effect of different volume fractions of the three-component system on the rheological properties was studied systematically (**Figure 2**). Capillary suspensions are generally obtained by a marginal addition of a secondary fluid, which strongly affects the rheological behaviour.[36] This is indeed the case for our system. For instance, adding 1 vol% PP to PDMS containing 12.4 vol% fumed silica creates an ink with *G'* exceeding *G″* in the linear viscoelastic regime (LVE) and a self-supporting yield stress (Figure 2a,b). The volume of PP relates to the liquid volume of PDMS and PP:

$$\left(vol\,\%_{PP} = \frac{V_{PP}}{V_{PDMS} + V_{PP}} \right) \tag{1}$$

while the silica volume relates to the overall volume

$$\left(vol\,\%_{SiO_2} = \frac{V_{SiO_2}}{V_{PDMS} + V_{PP} + V_{SiO_2}} \right) \tag{2}$$

In contrast, an ink without the PP behaves predominantly as a liquid with G″ large than *G'* within the LVE (Figure 2a,c).

An ideal rheological profile for DIW inks includes significant elasticity, as characterized by the value of the modulus or yield stress (characterized by amplitude sweep and shear rate sweeps), significant shear thinning (characterized by index *n* of Herschel-Bulkley fit), and fast thixotropic recovery (characterized by 3iTT). These effects were investigated for inks with PP content ranging from 1 to 40 vol% (Figure 2a–g). The shifts in rheological behaviour are significant, with a change of up to four orders of magnitude, e.g. the plateau storage modulus (Figure 2a) increases from 0.008 ± 0.001 kPa with no PP, over 0.626 ± 0.011 kPa (1 vol.% PP), 4.900 ± 0.152 kPa (15 vol.% PP) and 37.107 ± 1.147 kPa (30 vol.% PP) up to 82.872 ± 1.142 kPa (40 vol.% PP). The increase in elasticity is important for supporting the weight of the new lines deposited on top of the previous structure during DIW 3D printing.[28] Generally, a plateau storage modulus of 10 kPa and above is targeted for sufficient stability.[7,27,28] The increase in elastic response, *G'* and the yield stress can also be observed in the rise in static yield-stress (Figure 2b). The fitted lines in Figure 2b and static yield-stress values were obtained by a Herschel-Bulkley (HB) fit $\tau = \tau_0 + k \cdot \dot{\gamma}^n$, where τ is the shear stress, τ_0 is the static yield stress, k is the consistency index, $\dot{\gamma}$ is the shear rate and n is the flow index for the inks with PP. Whereas, linear region of inks without PP where fitted with a power-law fit $\tau = k \cdot \dot{\gamma}^n$. The wall slip affected region (crossed-out data points in Figure 2b) is omitted from the fit, as well as data that shows fracturing or possibly, shear banding (empty data points in Figure 2b). The wall slip affected

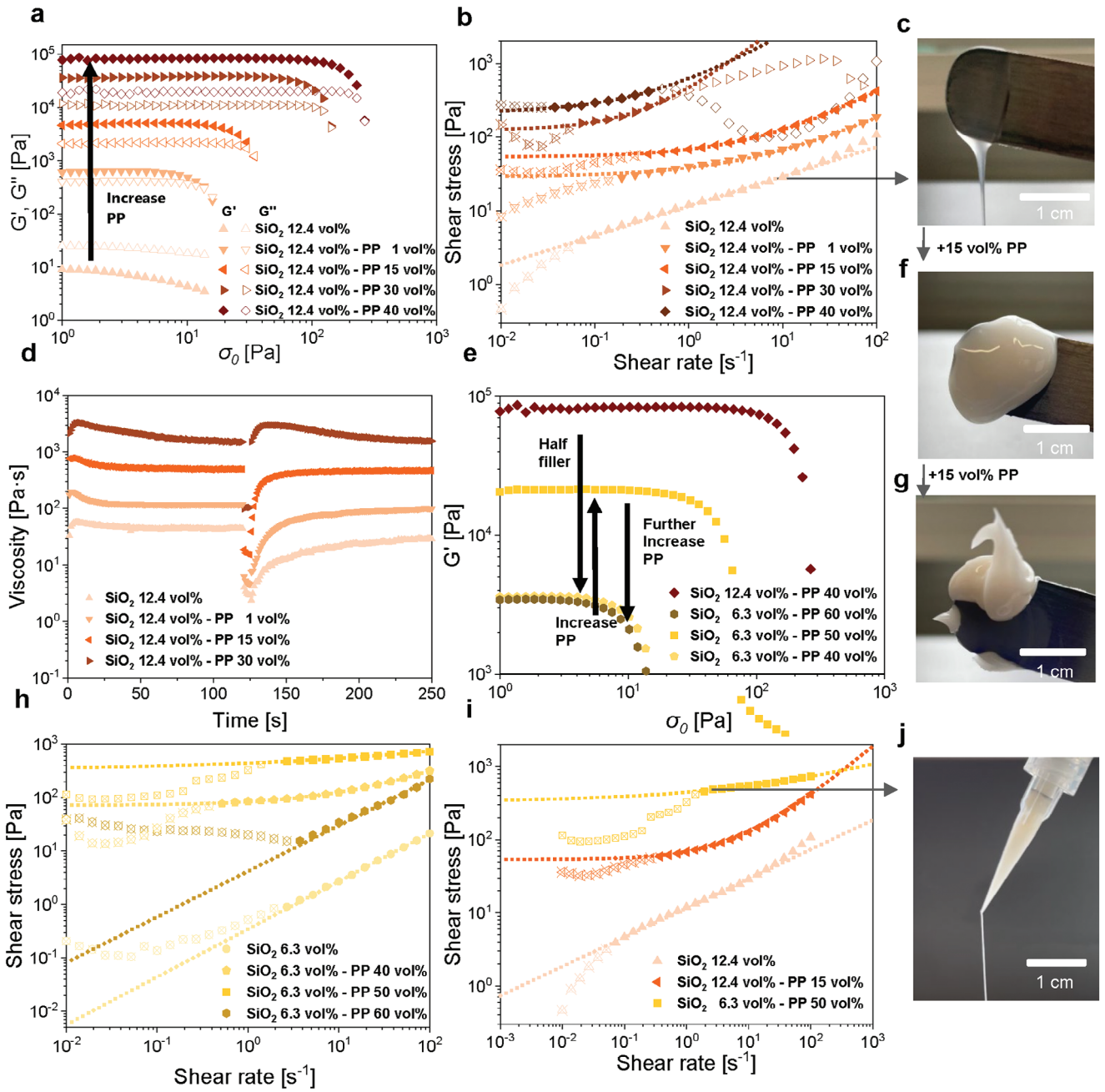

Figure 2. Rheological properties of the inks at varying silica and PP volume fractions. a) Stress-controlled amplitude sweep at 10 rad s^{-1}; b) Shear rate sweeps and Herschel-Bulkley & power-law fit (dotted lines), wall slip affected region indicated by crossed-out symbols and shear banding by empty symbols; c) Image of 12.4 vol% silica in PDMS; d) Three-interval thixotropy test (3-iTT) at intervals of at 0.1, 10, and 0.1 s^{-1}; e) Stress controlled amplitude sweep at 10 rad s^{-1} of varying silica and PP concentration; f) Image of 12.4 vol% silica in PDMS with 15 vol% PP; g) Image of 12.4 vol% silica in PDMS with 30 vol% PP; h) Shear rate sweeps of inks with 6.3 vol% silica and varying PP concentrations; i) Shear rate sweeps and Herschel-Bulkley & power law fits of ink with no PPs and 12.4 vol% silica, 12.4 vol% silica and 15 vol% PP and 6.3 vol% silica with 50 vol% PPs; j) Extrusion through a 200 µm nozzle of the ink containing 6.3 vol% silica and 50 vol% PP.

region was identified by performing shear rate sweeps with two differently hatched cone rheometer geometries (Figure S4a, Supporting Information). While sample fracturing can lead to similar drops in shear stress at shear rates above 1 s^{-1}, it is likely that the drop is a result of shear banding as the measurements were repeatable (Figure S4b, Supporting Information). Through the addition of PP the inks turn from a liquid with no static yield stress (no PP, power-law fit, $G'' > G'$ (LVE)) to weak gels with a static yield stress of 28.9 ± 2.4 Pa (1 vol.% PP, HB fit, $G'' > G''$ (LVE)), 53.8 ± 1.3 Pa (15 vol.% PP, HB fit, $G'' > G'$ (LVE), Figure 2f) and strong gels with 124.3 ± 31.1 Pa (30 vol.% PP, HB fit, $G'' > G''$ (LVE), Figure 2g) and 209.9 ± 20.5 Pa (40 vol.% PP,

HB fit, $G'' > G''$ (LVE)). The dynamic yield stresses, more precisely the perturbative yield stress, calculated as the shear stress value corresponding to when G' reaches 90% of G' at LVE, follow the same trend as the static yield stresses. While the ink with 12.4 vol% silica and no PP does neither possess a static nor a dynamic yield-stress, the inks with PP have a dynamic yield stress of 7.8 ± 0.4 Pa, (1 vol% PP), 16.7 ± 1.1 Pa (15 vol% PP), 64.3 ± 5.2 Pa (30 vol% PP) and 102.9 ± 5.1 Pa (40 vol% PP). While the trend is the same, the dynamic yield stress values are consistently lower than the static ones. A detailed overview of the fitted data and all resulting rheological values can be seen in Tables S1–S3 (Supporting Information). The yield stress is important to retain the shape after extrusion from the nozzle and is generally targeted for DIW to be above 100 Pa.[7,27,28] While our inks roughly reach these values, our calculations and difference between the dynamic and static yield-stresses show these values are a practical guide to simplify ink formulations, but printable inks can possess lower yield-stresses.

The recovery behavior after shearing is also relevant for DIW, as a fast recovery of the original modulus is needed for the deposited filament to contain its desired shape after exiting the nozzle. A three-interval thixotropy test (3iTT), mimicking the printing process by shearing at the first low shear interval with 0.1 s^{-1} for 120 s, second a high shear interval with 10 s^{-1} for 5 s, and the third low shear interval at 0.1 s^{-1} for 360 s, shows that the recovery speed in the third zone increases by increasing the PP concentration (Figure 2d). While the ink without PP takes 235 s to recover 90% of the viscosity, the ink with 1 vol% PP requires less time of 159 s and the ink with 15 vol% PP requires only 47 s; however, this time is still not fast enough for DIW. The ink with 30 vol% PP recovers 100% of its initial viscosity immediately (first measured data point, <1 s) and is ideal for DIW. Controlling the thixotropy is important for many printing processes, such as screen-printing, to achieve a high-resolution print.[44,45] Hence, the three-phase formulation can not only be used for DIW printing but is easily transferred to other printing and processing techniques where the ability to adjust both the particle and PP concentration provides a simple way to achieve a wide range of desired rheological properties.

While the ink filled with 12.4 vol% silica and 30 vol% PP is readily printable, the degree of shear thinning for all four inks with 12.4 vol% silica and various fractions of PP is not very high with a HB index n between 0.61–0.73. Stronger shear-thinning inks build up less pressure and can be more easily extruded through thinner nozzles and channels. By decreasing the fraction of silica, the degree of shear thinning can be increased, however, the elastic response decreases as well. Decreasing the silica concentration by half, from 12.4 to 6.3 vol.% at 40 vol.% PP reduces the plateau storage modulus (Figure 2e) from 82.87 ± 11.42 to 3.61 ± 0.02 kPa, respectively. The static yield stress (Figure 2b,h) decreases in line from 209.9 ± 20.5 Pa (12.4 vol.% silica, 40 vol% PP) to 72.82 ± 0.02 Pa (6.3 vol% silica, 40 vol% PP). As the dynamic yield stress and storage modulus are on the lower limit of suitability for DIW, an increase of the PP to 50 vol.% increases the storage modulus and the yield stress to 21.29 ± 0.12 kPa and 331.1 ± 42.9 Pa, respectively (Figure 2e,h; Video S1, Supporting Information). A further increase in PP to 60 vol.% led to an unstable suspension (Figure 2e,h; Figure S5, Supporting Information) that formed aggregates during shearing. Similar behavior has been reported for various other capillary systems and is attributed to the point where the secondary liquid becomes the dominant liquid, leading to a network rearrangement from a capillary to a pendular state.[46]

The range of printable suspensions was thus identified. While the further increase in PP leads to unstable suspensions, a further decrease in silica leads to an elastic response that is too low to be used for complex 3D structures created by DIW. A minimal silica concentration of 6.3 vol% is the lowest silica concentration needed to create strong enough gels for DIW. The filler loading is lower than most previously reported DIW printable capillary suspensions, where filler loadings with >10 vol% are usually employed.[32,36,38,47] The fact that such a low silica loading is sufficient to reach a printable percolating network stems from an interplay between multiple effects, specifically the degree of the immiscibility of the liquids, the affinity of the liquids to the filler, and the resulting contact angle. The surface roughness and available surface area of the particles as well as the viscosity of the two fluids, also play a role.[46]

Lastly, the overall advantages of adding PP to increase processability can be seen in Figure 2i. The addition of PP leads to an increase in elastic response, while the degree of shear thinning can be optimized by simultaneously decreasing the silica filler concentration to 6.3 vol% (Figure 2f,h,i). This ink showed a very high degree of shear thinning with a power law index n = 0.28 ± 0.05 combined with an elastic response high enough for DIW printing. The static yield stress and the degree of shear thinning are higher for this formulation (Figure 2i) than an ink containing 12.4 vol% silica, 12.4 vol% silica, and 15 vol% PP but also higher than for an ink with 22.5 vol% silica and no PP (Figure S6, Supporting Information). Additionally, an ink with 6.3 vol% silica and 100 vol% PP exhibits a lower static yield-stress of 66.7 ± 0.7 Pa and significantly lower degree of shear-thinning of n = 0.72 ± 0.00 (Figure S7, Supporting Information) compared to the ink with 6.3 vol% silica and 50 vol% PP. This showcases that through the polar-non-polar phase separation, rheological properties can be achieved that cannot be obtained through a single-phase system at these low filler concentrations. Consequently, adding PP reduces over 70% of silica in the formulation while giving more freedom in designing the ink compositions.

Capillary suspensions with immiscible polysiloxanes enable easy tuning of ink rheology parameters. By tuning silica and PP concentrations, a wide range of inks with varied shear thinning, viscosity, and elastic properties (yield stress and moduli) can be achieved. This flexibility in the ink design allows for the preparation of inks with tailored rheological behavior suitable for various printing techniques. Higher concentrations of silica and PPs have a similar, but not identical, impact on rheology, with the potential for the PP phase to become dominant. Moreover, the method developed here can easily be transposed to other formulations, e.g., commercially available silicone formulations, and adjusted to suit other processing techniques. We tested multiple commercially available formulations, such as Elastosil 604 RT, Sylgard 184, Sylgard 186, and Ecoflex 10. Strong rheological shifts could be observed for all formulations by adding PP (Figure S8, Supporting Information). DIW printable inks can be created solely by adding PP, removing the need to add further filler to these widely used formulations, as the fillers already present in the formulation are sufficient to achieve printable inks.

2.2. Elastomer Electromechanical Properties

The addition of PPs to a PDMS matrix offers a range of benefits beyond tunable ink rheology and enhanced processability. As mentioned previously, thermosets suitable for direct ink writing (DIW) typically exhibit high moduli (> 1 MPa) and significant viscous losses (> 0.1 tan(δ)), along with pronounced frequency and strain-dependent behavior due to the Mullins and Payne effects. These elastomer properties are unfavorable for applications requiring DETs. However, incorporating PP through a capillary suspension addresses these issues while also improving the mechanical and dielectric characteristics of the cross-linked elastomer. The greatest impact results from the reduced amount of silica compared to other printable polysiloxanes. Fillers reinforce the matrix and create a higher Young's moduli and, unfortunately, also increase mechanical losses, since fillers are non-elastic and convert mechanical energy into thermal energy through friction with each other and the elastomeric network. This loss is undesired, especially in repeated fast cyclic operations such as in DET, where the conversion of mechanical into thermal energy can heat the device. Generated heat deteriorates the electrical properties, such as the dielectric breakdown field, leading to accelerated aging. Consequently, a low amount of filler is desired for soft and highly elastic elastomers with low mechanical losses. To illustrate the impact of the silica in the formulations, three printable inks with optimized rheological behaviors are compared (**Figure 3**). The first has 1 vol% PP and 17.1 vol% silica, the second contains 30 vol% PP and 12.4 vol% silica, and the last has the highest PP content of 50 vol% and the lowest silica content of 6.3 vol%.

By decreasing the silica content while simultaneously increasing the PP content, the Young's modulus ($Y_{10\%}$) of the cross-linked elastomer decreases from 2.381 ± 0.01 MPa, over 1.275 ± 0.014 MPa, to 0.502 ± 0.004 MPa (Figure 3a,b). The cyclic stress-strain curves also show that Mullins effect and the hysteresis loop between each cycle are reduced by decreasing the silica concentration (Figure 3a,b). The elastomer containing 6.3 vol% silica and 50 vol% PP shows a significantly reduced Mullins effect and no noticeable hysteresis loops between cycles, which is unusual for polysiloxane elastomers processed by DIW. Besides, the Payne effect is significantly lower, as seen in the strain amplitude sweep measurement (Figure 3c). The reversible strain softening is mainly attributed to filler-filler interactions, which are decreased at higher strains. As a result, a lower silica content decreases the interactions in the elastomer. This leads to an obvious decrease in the storage modulus at higher strains, as observed in all samples (Figure 3c). The Payne effect causes a significant variation in tan(δ) across the measured strain and frequency ranges, particularly for high silica concentrations (17.1 and 12.4 vol%) (Figure S9, Supporting Information). However, the ink containing 50 vol% PP and 6.3 vol% silica shows small variations of the tan(δ) of only ± 0.01. Reducing the silica fraction decreases the modulus, hysteresis loop, and the Mullins and Payne effects and substantially decreases the mechanical loss modulus across all strain and frequency ranges. The mechanical losses for the sample with 17.1 vol% silica and 1 vol% PP are between tan(δ) of 0.09-0.12 are almost double the losses of the sample with only 6.3 vol% silica with a tan(δ) between 0.05–0.06. The sample with 12.4 vol% silica and 30 vol% PP is between the two with a tan(δ) range of 0.075-0.11. In contrast to the strain amplitude sweep, the frequency sweep (Figure S10, Supporting Information) shows a typical stiffening effect of elastomers with increased frequency. Again, the mechanical losses remain rather constant for the lowest silica concentration with values of 0.05 ± 0.01 (Figure S9, Supporting Information), where the losses decrease significantly with higher frequencies for the elastomers with higher silica loadings. At higher frequencies, the increase in stiffness of the polymer chains leads to decreased losses. While this could be advantageous in reducing losses in DET applications, the strong increase in modulus would significantly change the operation conditions. The storage modulus of the elastomers with the highest silica concentrations increased from 0.05 to 10 Hz by 1.4 MPa (≈45% increase). The elastomer with 12.4 vol% silica concentration showed an increase in storage modulus of 0.6 MPa (≈50% increase), while the elastomer with the lowest silica concentration showed an increase in storage modulus of only 0.13 MPa (≈25% increase) over the same frequency range. We further optimized the elastomer with the lowest silica content by varying the cross-linker concentration (Figure 3d,e,f). With a higher cross-linker concentration, the modulus was increased to 917 kPa, while the loss factor stayed almost constant (Figure 3f). By decreasing the cross-linker concentration, Young's modulus dropped to 265 kPa, however, the elastomer's losses are increased to a tan(δ) of ≈0.1 (Figure 3f). While the tan(δ) increase is not desirable, it is lower than other printable elastomers, especially considering the low modulus of the elastomer.[10] Swelling experiments with THF (20 mL g^{-1}) showed that a large part of the PP remains as a softener in the elastomer. About 58.01 ± 0.40 wt.% remained in the network, while 41.99 ± 0.40 wt.% were extracted. This is comparable to similarly soft commercially available formulations such as Ecoflex 50, 30, or 10. NMR analysis showed that ≈9% of the leached fraction was PDMS, and the main part with 91% was PP (Figure S11, Supporting Information). Assuming no particles could be extracted, only ≈17 % of the total PP remained in the elastomer after extraction. This suggests some PP cross-links within the elastomer, but most do not. It appears likely that only the interfaces between PP and PDMS cross-link as the non-polar crosslinker is not soluble in the PP phase and only comes in contact on the interfaces with the crosslinker. Reducing the sol fraction would consequently require the use of an additional, polar miscible cross-linker.

The strain at break increases from 100% to 170% maximum strain in line with the losses and decreasing cross-linker concentration. As a result, the elastomer with the lowest silica content and moderate crosslinker amount exhibits a distinct combination of DIW printability, softness, low mechanical losses, minimal Mullins and Payne effects, and low hysteresis. Remarkably, as shown in Figure 3a, this elastomer achieves the desired ranges for all the mechanical parameters outlined for DEAs by Madsen et al.[25] This achievement is noteworthy, considering the challenge of simultaneously achieving these parameters, even for elastomers that are not DIW printable. Besides the mechanical properties, adding PP also increases the dielectric permittivity of the cross-linked elastomer, as PP has a relative permittivity of 18.16 ± 1.50 (Figure S3, Supporting Information). The relative permittivity increases from 3.43 ± 0.02 (1 vol% PP), over 6.72 ± 0.10 (30 vol% PP), to 11.39 ± 0.36 (50 vol% PP) at 100 Hz (**Figure 4**). The increase in permittivity is due to the orientation

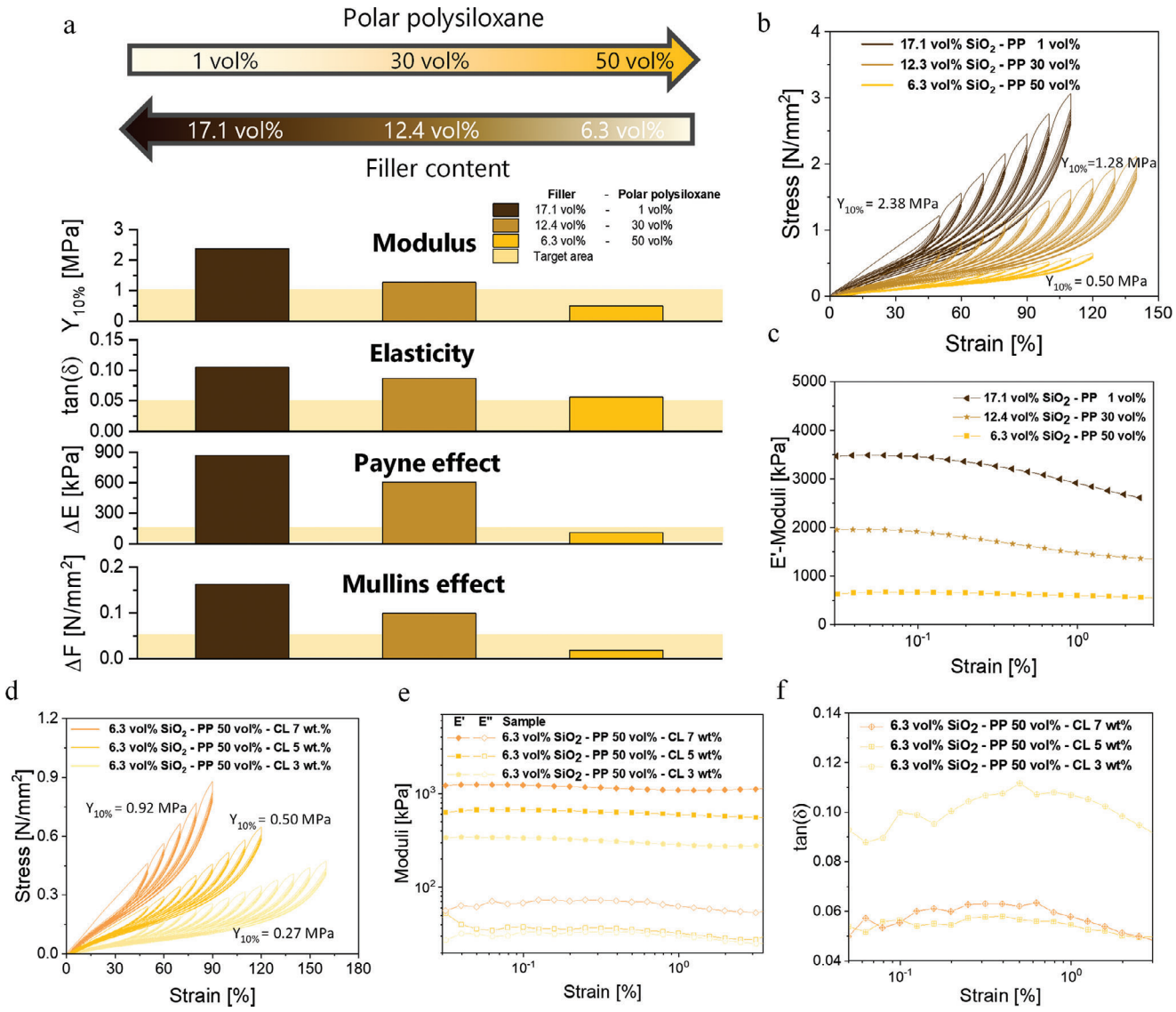

Figure 3. Mechanical analysis of elastomers with similar DIW printability but three different silica and PP concentrations. a) Impact on simultaneously changing silica and PP concentrations on mechanical parameters such as modulus, tan (δ), Payne & Mullins effect. b) Cyclic stress-strain curves of samples with different silica and PP content. c) DMA storage modulus of strain sweep. d) Cyclic stress-strain curve of elastomers with the lowest silica concentration and varying cross-linker content. e) DMA storage and loss modulus of strain sweep of elastomers with the lowest silica concentration and varying cross-linker content. f) Loss tangent of the storage and loss modulus of strain sweep of elastomers with the lowest silica concentration and varying cross-linker content.

polarization of the nitrile groups, which occurs at frequencies up to 1 MHz. The conductivity increases along the permittivity, which is a well-reported phenomenon.[17] Nonetheless, the ion conductivity is still between 10^{-13}–10^{-11} S cm^{-1} and is thus in a typical range of dielectric insulators.

The dielectric losses increase with permittivity and are frequency-dependent. At AC frequencies below 100 Hz, the losses due to electrode polarization are similar for all samples. The losses are rather small at frequencies between 1 and 100 Hz, which is the most interesting window for the operations of DEA. At higher frequencies (10^2–10^4 Hz), the dielectric losses increase again. The relaxation times follow a VFT-fit with a T_g of −52.40 °C (Figures S12 and S13, Supporting Information). This suggests that the process results from the dipole alignment of the polar phase present at the interfaces. Significant differences in the dielectric losses of different elastomers can be observed at frequencies ≈1 kHz. However, most DET applications will not be used at frequencies above 1 kHz. Since real capacitors always consist of a resistive and capacitive part, the phase angle is a measure to determine if the elastomer predominantly acts as a capacitor ($\phi = -90°$) or resistor ($\phi = 0°$). All three elastomers exhibit the behavior of good capacitors with low resistive losses and phase angles ($\phi < -88°$) until electrode polarization sets in at frequencies below 1 Hz. Surprisingly, all three elastomers have similar phase angles over the whole frequency range, except for the dipole alignment process predominantly occurring between

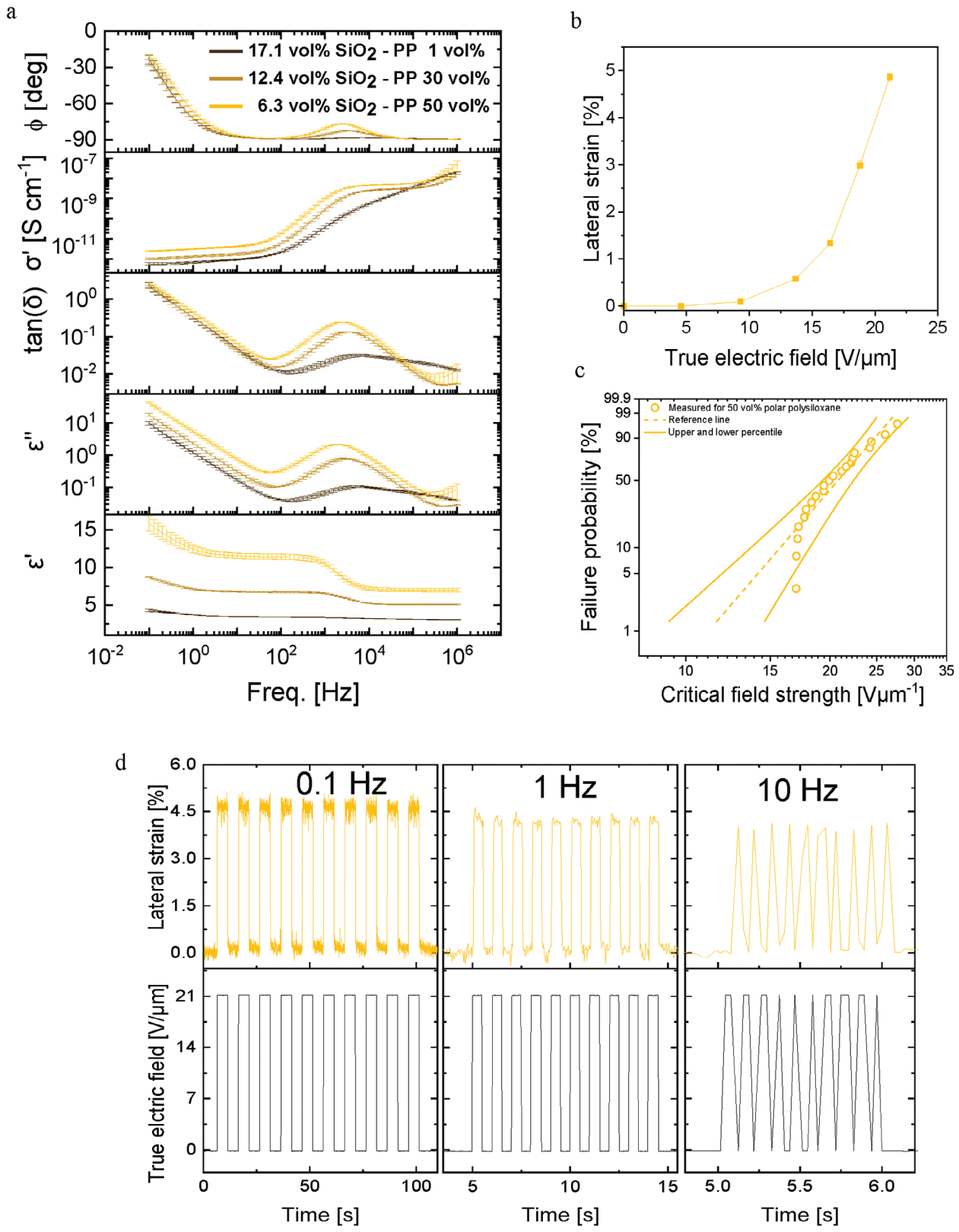

Figure 4. Dielectric characterization a) Dielectric spectroscopy investigations of dielectrics with varying PP and silica concentrations. b) Lateral actuation of a single-layer elastomer actuator with 50 vol% PP and 6.3 vol% silica at 1 Hz. c) Breakdown field probability of an elastomer with 50 vol% PP and 6.3 vol% silica d) Actuation of an elastomer with 50 vol% PP and 6.3 vol% silica at frequencies of 0.1, 1, and 10 Hz. The data points for 10 Hz are not smooth due to the optical camera system's maximum sampling frequency of 30 Hz, resulting in only three data points per cycle.

1 and 10 kHz. This contrasts previous works on PP, where increased PP often leads to higher capacitive losses.[21,26] Creating a discontinuous phase through the capillary suspension might be responsible for decreasing capacitive losses. This approach could have far-reaching implications, as most polar polymers suffer from high capacitive losses, which might be significantly improved by adding a small amount of silica and PDMS and creating capillary suspensions.

Due to the high permittivity and the low modulus, the single-layer actuator responds at a low electric field: actuation is observable between 11–22 V μm^{-1} (Figure 4b). The major drawback of high-permittivity polymers is the reduced dielectric breakdown field, which is significantly lower than commercial PDMS with ≈50–70 V μm^{-1} (Figure 4c).[18,21,22,26] The critical breakdown strength of the new elastomer is lower than PDMS, but higher compared to previously reported polysiloxane composites with similar high permittivity.[48] The electrical breakdown field was 21.93 ± 1.57 V μm^{-1} with a Weibull form factor of 6.80. High-permittivity polysiloxanes lead to actuation at lower electric fields, but suffer early dielectric breakdown. While the lower breakdown field adversely impacts the energy density, the increased permittivity improves the energy density. We note that the probability of a breakdown highly depends upon measurement conditions such as humidity, temperature, and processing.[49] Therefore, direct comparisons with other elastomers must be made cautiously. The low viscous losses and elasticity of the dielectric were further confirmed by the actuation strain, which was independent of the actuation frequency (Figure 4d). At 21 V μm^{-1} the dielectric has a lateral actuation strain of 5%, that stays constant at 0.1, 1, and 10 Hz.

The unmatched formulation of DIW printable inks enables the creation of soft elastomers with remarkable properties: high dielectric permittivity and low mechanical losses. What is very remarkable is that these superior characteristics can be achieved by simply blending three different components. One of these components, PP, serves multiple purposes, acting as a high-permittivity thixotropic softener. As we proceed, it is worth noting that both the ink and cross-linked elastomer consist of 50 vol% PP, 6.3 vol% silica, and 5 wt.% cross-linker. These specific ratios have been carefully selected to ensure optimal rheological ink and electromechanical elastomer properties, which are crucial for the success of DIW and subsequent device operation.

2.3. DIW of Capillary Ink and Multimaterial Printing

To demonstrate the utility of the capillary formulations witoptimized rheological and electromechanical properties, we 3D printed the inks into various arbitrary structures, created a compliant electrode ink, and used multimaterial printing to achieve layered dielectric elastomer actuators (**Figure 5**). The capillary ink was used to print complex structures, including hollow cylinders, layered grid structures, hollow cones, and hollow cubes (Figure 5a). Due to the high degree of shear thinning, the ink was printed with a comparatively low pressure of 0.7 bar and 22 mm^{-1} s with a nozzle of 400 µm. The image of the nozzle during and after printing shows that the ink readily flows through the nozzle and the flow can be stopped without leaving threads at the nozzle. As described previously, the strong shear thinning behavior of the ink allows easy and accurate printing and process control. The printed and cured structures possess excellent deformability in all three dimensions due to their softness. These elastomer structures regain their original shape after the applied stress is removed, owing to their remarkable elasticity and minimal mechanical losses. This combination of properties allows for printing structures with overhangs and unsupported designs, as exemplified by the hollow cone and grid structures (Figure 5a).

An electrode ink is also needed to create stack DEA by multimaterial 3D printing. The electrode ink was prepared with different weight ratios of carbon black in PDMS from 10 wt.%–15 wt.%. All three inks show strong shear thinning (Figure 5c), and the static yield stress of 12.5 wt.% CB ink is 364.2 ± 4.2 Pa (Figure S14, Supporting Information). This is commonly observed for carbon black, as the high surface roughness of carbon black (CB) particles can cause them to interlock and form strong gels.[9,10,50] The ink selected for multimaterial printing consists of a medium filler loading of 12.5 wt.% CB in PDMS, which readily holds its shape after extrusion (Figure 5b). The electrode ink is cross-linked in a post-processing step into an elastomer with the same crosslinking chemistry as the dielectric, whereby delamination of the printed structure during operation is prevented by the covalent bonds at the electrode/dielectric interfaces. The conductivity of the electrode is 3.02 10^{-4} ± 3.8 10^{-5} S m^{-1} (Figure S15, Supporting Information). The electrode elastomer has a storage modulus E' of 1.58 ± 0.06 MPa and a low tan(δ) of 0.029 ± 0.002 (Figure S16, Supporting Information, 0.05 to 10 Hz at 2% strain). While the low tan(δ) is favorable for DEA operations, the high modulus is not, as the electrode is passive and restricts the actuator movement.

The multimaterial printhead alternates between the electrode ink (12.5 wt.% CB) and the capillary suspension dielectric ink (Figure 5c). To decrease defects during printing due to unstable flows at the start (pre-flow) and the end of the extrusion (post-flow), the printing path was designed to have the start and end points in inactive regions outside the stack. The first layer is the electrode, the second is the dielectric active layer, and the third is the electrode. The images (Figure 5c) show the printing process of the first three layers. The electrode, dielectric, and opposite electrode printing steps can be repeated multiple times to build up a stack DEA with a different number of active layers (Figures S17 and S18, Supporting Information). The whole printing process can be seen in Video S2 (Supporting Information). Every other electrode layer is connected on the side of the stack. On all sides, the stack actuator has inactive parts that prevent the oppositely charged electrodes from contacting (left and right sides of the stack) and avoid dielectric breakdowns through the air (front and back sides of the stack). On the side, every other electrode layer is printed so that an electrical connection is ensured. An image of the printing of the 23rd layer can be seen in Figure 5d, while the final, yet uncured 23-layer stack dielectric elastomer actuator is depicted in Figure 5e. After printing, the stacks were cross-linked at 80 °C for 16 and allowed to rest for at least two weeks before testing (Figure 5f).

The cross-linked stack was cut and imaged using an SEM and optical microscope (Figure 5g,h). Relatively consistent layers, no delamination, no voids, and a good, printed layers connection can be seen. By printing the lines close together and slightly over extrusion, the printed lines merge, making it impossible to identify

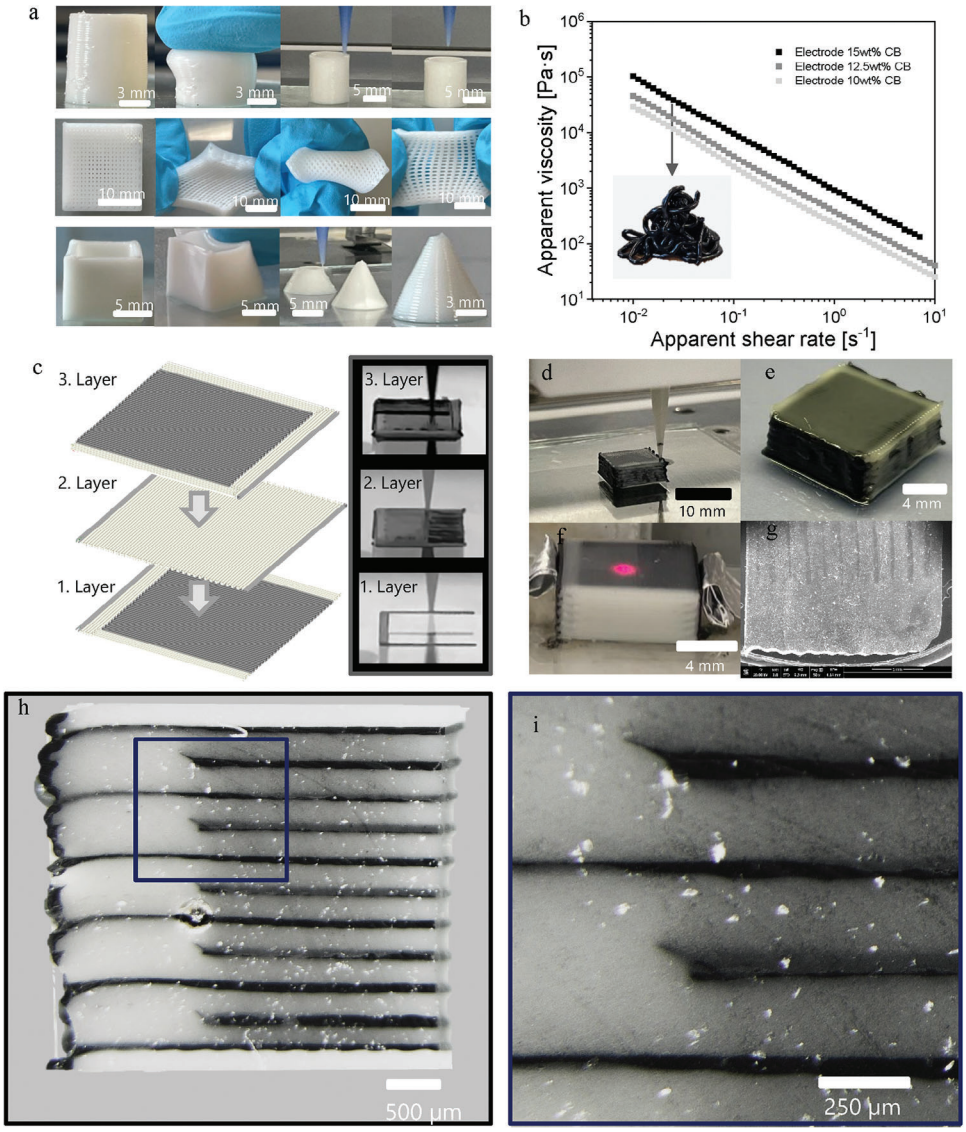

Figure 5. Printing of capillary inks, creation of electrode ink, multimaterial printing process and printed layered devices. a) Images of 3D printing of the capillary ink containing 50 vol% PP, 6.3 vol% silica, and 5 wt.% cross-linker, printed and cross-linked structures and their deformability from top to bottom: hollow cylinder, 20 layer grid, hollow cubes and hollow cones. b) Rheological characterization of the electrode inks shear rate sweeps, inset image of extruded ink. c) Printing paths and process for the electrode (grey) and dielectric (yellow) inks with images of the printing process. d) Last printing line of a 23-layer DEA. e) Image of a printed interdigitated stack dielectric elastomer actuator made from 23 layers in the uncured stade and f) the cured stade connected to Al electrodes. g) SEM image of a cut stack, the darker lines are the electrode layers while the bottom part is the passive dielectric area. h) Optical image of a printed, cured and cut 23-layer DEA with a dielectric breakdown at the 5th electrode. i) Zoom in on the whole stack to show four electrodes and five dielectric layers.

the single printing lines. The final printed stack's dimensions are 1 cm × 1 cm with a total height of 3.6 mm. The 23 layers consist of two insulating layers on the bottom and top and alternating dielectric/electrode layers. This configuration forms ten active capacitive layers. The active area of each capacitor is 8 mm × 6.8 mm. The stacks respond at relatively low voltages considering the thickness of the dielectric films of 210 µm, which is a constraint of the printing process (**Figure 6**). The contractile displacement in Figure 6a shows that the layered actuator follows the classical analytical model of quadratic dependence on the electric field. This is true independent of frequency at 1 and 100 Hz. The high bandwidth and low elastic losses of polysiloxane-based actuators enable the actuation even at 100 Hz. In fact, a resonance frequency close to 100 Hz leads to an increase in actuation compared to 1 Hz. The first actuation at 1 Hz could be measured at 2.3 kV, corresponding to 11 V µm^{-1} (Figure 6b). This value is in line with the single-layer actuator, where the actuation onset at 1 Hz is also at 11 V µm^{-1} (Figure 4c). These voltages and electric fields are lower than those reported for DIW printed actuators in the literature (4–12 kV or 26–58 V µm^{-1}).[10] An overview of previously printed DET is given in Table S4 (Supporting Information). These low electric fields are possible due to the

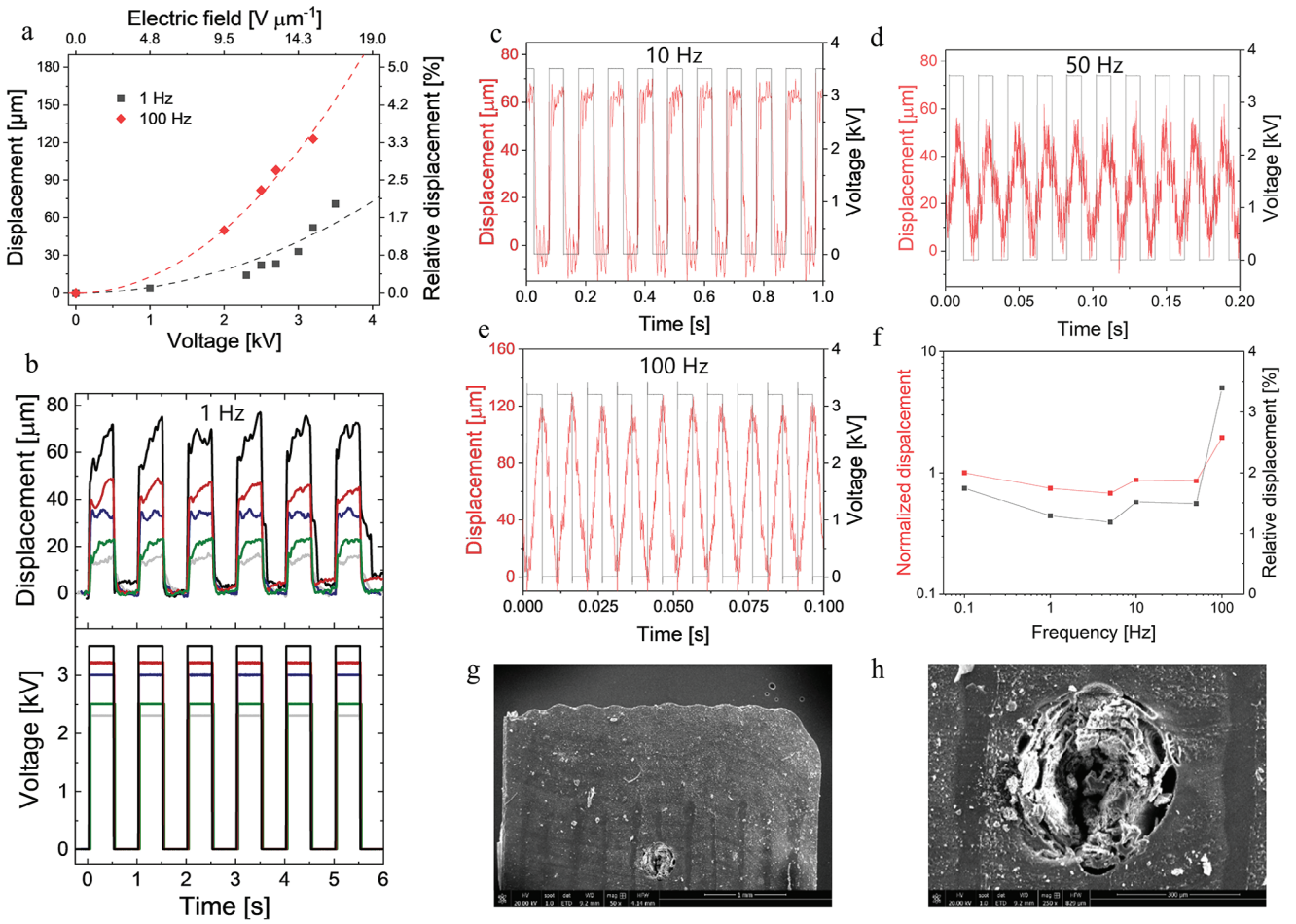

Figure 6. Actuation characterization of a fully printed 23 layers dielectric elastomer actuator with a high-permittivity dielectric. a) Absolute and relative contractile displacement as a function of voltage and electric field at 1 and 100 Hz with their respective quadratic fit functions. b) Voltage-dependent displacement at 1 Hz at 2.3, 2.5, 3.0, 3.2 and 3.5 kV. c) Actuation at 10 Hz and 3.5 kV d) Actuation at 50 Hz and 3.5 kV. e) Actuation at 100 Hz and 3.2 kV. f) Normalized and relative displacement as a function of frequency at 3.2 kV. g) SEM of a 23-layer printed dielectric elastomer actuator after an electrical breakdown. h) SEM image enlargement of an electrical breakdown.

combination of high permittivity and low elastic modulus of the dielectric caused by the addition of the PP. With increasing voltages, the actuation can be increased up to a displacement of 75 µm at 3.5 kV, equivalent to ≈17 V µm^{-1} at 1 Hz, corresponding to ≈2% actuation strain (Video S3, Supporting Information). The actuation is consistent and repeatable. Due to the high elasticity, increasing the actuation frequency leads to only a small decrease in actuation performance at 10 Hz (Figure 6c), with a displacement of 70 µm marginally lower, and immediately follows the applied square wave of the electric field (Video S4, Supporting Information). At 50 Hz (Figure 6d), the actuation drops to 50 µm (Video S5, Supporting Information) and the actuator requires ≈10 ms (or half the time the voltage is on to reach full actuation) and stays the other half of the time in the maximum actuation state. After switching off the voltage, the time needed to reach the fully discharged state is about the same as for achieving the full actuation. If the frequency is further increased to 100 Hz (Figure 6e), the time to reach the maximum actuation is 10 ms, the same as when the electrical field is turned on. Even though the actuator stays only for less than 1 ms in the maximum actuated state, the maximum strain increases significantly compared to lower frequencies. For example, at 3.2 kV and 100 Hz the total displacement reaches 123 µm or a relative displacement of 3.42 % compared to a total displacement of only 52 µm or 1.44 % at 3.2 kV and 1 Hz (Figure 6f). The actuation between frequencies from 0.1–50 Hz varies only slightly before it hits a resonance band at 100 Hz and increases again. The actuators where subjected to one million cycles at 3.5 kV and 100 Hz. The actuation strain reduced from 3.5% to 2.7% during the one million cycles (Figure S19, Supporting Information). At ≈3.8 kV the actuator experiences an electrical breakdown (Figure 6g,h). The first breakdown occurs at ≈18 V µm^{-1}, which is only 4 V µm^{-1} lower than the breakdown in a single layer. While the variation in dielectric film thickness of ± 10 µm may be responsible for the earlier breakdown, the stiffening effect of the electrode, due to the rather high thickness (110 µm) and modulus (1.58 ± 0.06 MPa), might also play a role. Additionally, defects between the layers may be created during the printing process and the switching between the two inks. Most breakdowns were observed close to the edges of the active layers. The printed layers tend to be

uneven and have defects at the start and end of printing paths as well as on the transition parts between the two inks, which can be observed in the slight upward fold of the electrode in the microscope image of Figure 5i. This inaccuracy is an inherent issue of the printing technique, which can only be overcome by co-extrusion processes.[4,10,11] The breakdown occurred at the edge of one of the middle layers of the printed structure. Typical for carbon black-based electrodes, the electrical discharge burns the surrounding dielectric.

3. Conclusion

We developed a straightforward and adaptable approach to formulate solvent-free capillary inks. The inks consist of polar and non-polar polysiloxane liquids with a small amount of silica filler and can be cross-linked into elastomers. The ink rheology and final elastomer properties can be more freely adjusted than for non-capillary polysiloxane suspensions. After printing, the two immiscible fluids are cross-linked to form elastomer networks. In contrast to conventional capillary inks, where at least one fluid evaporates post-printing, our approach uses two immiscible fluids that remain within the final printed structure. The cross-linking reaction chemically connects the different phases to form elastic networks with easily tunable properties. We achieve rheological properties ideal for DIW with a volume fraction of filler significantly lower than traditional inks. The minimally filled inks can be printed in different structures and shapes and then cross-linked into elastomers with a low Young's modulus and very low $\tan(\delta) = 0.05$. While the capillary ink formulation strategy allowed for printable soft elastomers, the PP content synergistically increased the dielectric permittivity of the composite. The ink exhibited good printability and was used to print fully layered dielectric elastomer actuators. After cross-linking, the printed structures actuated at rather low applied voltages, thus validating their potential for creating printed dielectric elastomer actuators. The durability of the printed actuator was proven through an extensive long-term cyclic load test, wherein a stack actuator underwent testing at 3.5 kV and 100 Hz for one million cycles. Therefore, we anticipate that this capillary ink strategy can be readily extended to incorporate other components. Since the secondary fluid serves as both a rheological modifier and an active ingredient in the final elastomer, we have significantly broadened the design space for capillary suspensions, opening new pathways to develop innovative functional materials and devices.

4. Experimental Section

Materials: 3-Cyanopropylmethyldichlorsilane, silanol-terminated PDMS (45–85 cSt), and (25%–35% methylhydrosiloxane-*co*-dimethylsiloxane) polymer (25 cSt), hexamethyldisilazane treated silicon dioxide (Figure S20, Supporting Information), and dibutyltin dilaurate (DBTL) were purchased from ABCR. $NaHCO_3$ was purchased from Sigma–Aldrich. Toluene and dichloromethane were purchased from VWR Chemicals. Carbon black 100% compressed from acetylene was purchased from Gelest. All reagents were used without further purification unless otherwise stated.

Synthesis of Polar Polysiloxane (PP): 3-Cyanopropylmethyldichlorsilane (120 mL, 138.05 g, 0.76 mol, 1 eq.) was added dropwise to a dispersion of $NaHCO_3$ (223 g, 2.65 mol, 3 eq.) in 1 L toluene. After the addition, the mixture was stirred at 110 °C for 12 h while removing water under azeotropic distillation. The reaction was filtered and washed with dichloromethane. The organic phase was washed with water three times, and the solvent was removed. After drying at 110 °C under vacuum, a yellowish, viscous liquid was obtained with a yield of 93%. ^{1}H NMR (400 MHz, $CDCl_3$) δ: 2.42 (m, 2H, CH_2-CN), 1.70 (m, 2H, CH_2-CH_2-CN), 0.75 (m, 2H, Si-CH_2), 0.15 ppm (m, 3H, Si-CH_3) (Figure S21, Supporting Information); ^{13}C NMR (100 MHz, $CDCl_3$) δ: 119.75 (CN), 20.55 (CH_2-CN), 19.82 (CH_2-CH_2-CN), 16.95 (Si-CH_2), −0.18 ppm (Si-CH_3) (Figure S22, Supporting Information). TGA (Δ = 1.5 wt.%) = 319.70°C (Figure S23, Supporting Information). M_n = 9.34 kDa; M_w = 14.10 kDa, PDI: 1.51. (Figure S24, Supporting Information); T_g = −59.27°C (Figure S25, Supporting Information); relative permittivity (1 V AC, $5{\cdot}10^5$ to $5{\cdot}10^4$ Hz): 18.16 ± 1.50 (20 °C), 7.39 ± 1.15 (−60 °C). Netownian fluid with a viscosity of 6.65 ± 0.08 Pa s (Figure S1, Supporting Information).

Capillary Ink Preparation: The silanol-terminated PDMS (45–85 cSt) (15 g) was mixed with surface functionalized hydrophobic silica (5 g) in a SpeedMixer for five minutes at 3500 rpm. In the next step, (25%–35% methylhydrosiloxane-*co*-dimethylsiloxane) polymer (0.675 g) with a viscosity of 25–35 cSt was added and mixed for 1 min at 3500 rpm in a SpeedMixer. Polar polysiloxane (17.45 g) was added and mixed for another 5 min at 3500 rpm in the SpeedMixer. Lastly, 200 µL of dibutyltin dilaurate (DBTL) was added and, for one more minute, mixed in the SpeedMixer at 3500 rpm. The ink was loaded into 30 cc syringes and trapped air was removed in a centrifuge at 6000 rcf for 10 min.

Conductive Ink: For the conductive ink, carbon black (5.7 g) was added to silanol-terminated PDMS (45–85 cSt) (38.4 g) and 5 min SpeedMixed at 3500 rpm. (25%-35% methylhydrosiloxane-*co*-dimethylsiloxane) polymer (1.6 g) was added to the ink and mixed for one minute at 3500 rpm. Lastly, DBTL (400 µL) was added and mixed in for one more minute at 3500 rpm in the SpeedMixer. The ink was three-roll milled five times and loaded into a 30 cc syringe. The syringe was centrifuged at 3000 rcf for 10 min.

Multimaterial Printing: Electrode and dielectric layered devices were manufactured with a direct ink writing printer (3D-Bioplotter "Manufacturer Series," EnvisionTEC, Germany). The ink was pneumatically extruded with pressures ranging between 0.3 and 1 bar, through conical nozzles with an inner diameter of 0.2 and 0.4 mm. The print head switched automatically between the two inks after completing each layer. The filaments were deposited on glass slides at speeds ranging between 10 and 25 mm s^{-1}. After printing, the produced parts were cured at 80 °C for 16 h and rested for at least two weeks before mechanical or electrical characterization and testing. For our stacks (23 layers, 10 × 10 mm), a total path length of ≈640 mm per layer was re-quired, resulting in a theoretical printing time per layer between 64 to 25.6 s and a total of 24.5 to 9.81 min print time for the complete stack. However, the 3D printer used is not ideal for multimaterial printing. The printer has only one print head and must repeatedly switch between the cartridges. Essentially, the switching time of the inks due to the printer layout became a major time constraint of the printing process. The real printing time took 40 min for a stack consisting of 23 layers, mostly due to the very slow switching between electrode and dielectric inks, which is the default setting of the printer. This could be significantly reduced without sacrificing accuracy if a second print head would be installed into the printer.

Rheological Characterization: Shear rate sweeps and three-interval thixotropy tests (3ITTs) of the different inks were performed on a MCR 502 rheometer furnished with a second (bottom unit) motor. This twin drive setup allows for performing rheological measurements with two torque transducers and two drive units at once. The measurements were performed in SMT (Separate Motor Transducer) mode: we employed a hatched, 4°, 25 mm diameter cone as the bottom driving geometry and a cross-hatched 25 mm outer diameter, 8 mm measuring diameter, partitioned plate as the upper measuring geometry. The partitioned plate geometry was employed to eliminate (or at least greatly reduce) the impact of edge fracture effects on the rheological measurements, as this can often impact measurements of high yield stress fluids at large deformations/rates. Rough geometries were utilized to diminish the effect of wall slip during the measurements. These measurements were conducted in a CTD 600 (Convection Temperature Device) at room temperature. Shear rate sweeps from 0.01 to 100 s^{-1} were conducted in logarithmically spaced

steps (7 points/decade) with durations ranging from 200 to 10 s to guarantee that the samples were in a steady state during data acquisition. Despite the use of rough geometries, wall slip-related artifacts can be observed at low shear rates (≈0.01 to 0.5 s^{-1}), in this region, the measured shear stress is strongly underestimated and departs from the Herschel-Bulkley and power law fits. To confirm that these are wall slip artifacts, we repeated shear rate sweeps on the 12.4 SiO_2 vol%, 40 polar poly-siloxane vol% ink with a hatched, 8.5°, 25 mm diameter cone (Figure S2a, Supporting Information): the wall slip affected region of the data is lesser when using a higher degree cone (analogously to using higher measuring gap in plate-plate measurements.[51] Moreover, data collected at very low shear rates should be excluded from the analysis, as the samples did not reach a steady state in the waiting time for shear stress data acquisition, as shown in the flow start-up measurements (Figure S26, Supporting Information). This portion of data was hence excluded from the fits. The shear rate sweeps of samples that showed $G'>G''$ in the LVE (Linear Viscoelastic Regime) in amplitude sweep measurements were fit to the Herschel-Bulkley model: $\tau = \tau_y + K \cdot \dot{\gamma}^n$ (with τ: shear stress [Pa], τ_y: yield stress [Pa], K: consistency index [Pa·s^n], $\dot{\gamma}$: shear rate [s^{-1}] and n: flow index [-]). The two samples (6.3 SiO_2 vol%, no polar poly-siloxane vol% and 12.4 SiO_2 vol%, no polar poly-siloxane vol%) that showed $G''>G'$ in the LVE in amplitude sweep measurements were instead modeled as simple power law fluids: $\tau = K \cdot \dot{\gamma}^n$ (with τ: shear stress [Pa], K: flow consistency index [Pa·s^n], $\dot{\gamma}$: shear rate [s^{-1}] and n: flow behavior index [-]). Fits, models' R^2 values and standard deviation of parameters were computed on MATLAB. Three Interval Thixotropy Tests (3ITTs) were performed with the following protocol: first, the samples were sheared at 0.1 s^{-1} for 120 s, then immediately at 10 s^{-1} for 5 s and then at 0.1 s^{-1} for 360 s (data acquisition: 1 pt s^{-1}). Recovery of the viscosity after high shear rate interval was tracked and the time to recover 90% and 100% of the equilibrium viscosity (viscosity at the end of the first low shear rate interval) was extrapolated.

Amplitude sweeps and flow start-ups were performed on a single motor, stress-controlled, MCR 502 rheometer coupled with a Peltier temperature control unit set at 25 °C. For these measurements, we employed a hatched, 4°, 25 mm diameter cone geometry and a 25 mm diameter hatched bottom plate (fastened to the Peltier unit). Amplitude sweeps were performed at an angular frequency of 10 rad s^{-1}, shear stress was ramped in logarithmically spaced steps (15 points/decade) from 0.1 to 500 Pa. The dynamic yield stress $\tau_{y,dyn}$ was extrapolated by taking the shear stress value corresponding to when the measured storage modulus drops below 90% of its LVE (Linear Viscoelastic Regime) plateau value.[52] Flow start-ups were performed on 6.3 SiO_2 vol%, 50 polar poly-siloxane vol% and 12.4 SiO_2 vol%, 1 polar poly-siloxane vol% inks. The samples were sheared at a constant shear rate of 0.01 s^{-1} (the lowest shear rate value in shear rate sweeps) for 1 h, and the shear stress was measured to observe when the samples reached a steady–state (Figure S26, Supporting Information).

Tensile Measurements: Tensile measurements were performed with a Zwick Z010 tensile test machine with a 50 mm min^{-1} speed using dog-bone-shaped samples of 18 mm length and 2 mm width. The Young's moduli were determined from the linear fit slope of the stress–strain curves from 0 ≤ 10%.

Dynamic Mechanical Analysis: Dynamic mechanical analysis (DMA) was carried out on an RSA 3 DMA from TA Instruments in the tensile mode. Stripes of samples with rectangular geometry (10 mm by 30 mm) were measured under a dynamic load of 2 g. Data in the frequency sweeps were obtained by applying 2% strain in the frequency range of 0.05–10 Hz. The amplitude scans were performed at 0.1 Hz from 0.05% to 10% strain.

Broadband Dielectric Spectroscopy: Temperature-dependent dielectric properties were evaluated using a Novocontrol Alpha-A Frequency Analyzer equipped with quatro cryosystem temperature control. Dielectric spectra were recorded by applying an external voltage of 1 V in an AC frequency range of 0.01 Hz to 1 MHz at RT and between −155 and +110 °C.

Dielectric Breakdown Measurement: A 12.5 kV DC high voltage power supply system (HCL 35–12500 pos, *FUG electronic GmbH*, Germany) was used for all measurements. Samples were sandwiched between two metal electrodes with 1 mm^2 area embedded in an epoxy resin. The applied voltage was linearly increased until failure voltage was recorded on several samples. Statistical analysis was employed to evaluate the dielectric breakdown field, commonly following the Weibull probability model.

Actuation Tests: Electromechanical tests were performed with circular membrane actuators. The polymer films were fixed between two circular frames after applying a biaxial pre-stretch of 7.4%. The pre-stretch was used not to reach a specific strain level in the material but rather to fix the film reliably between the rigid frame to prevent it from buckling or sagging. We thereby aim to have a low pre-stretch to be as close as possible to a free-standing, unstrained film but still be able to measure the strain level with the optical camera accurately. Carbon black powder was applied on each side of the film with a brush as circular electrodes. The electrodes were connected to a FUG HCL-35-12500 HV power supply with aluminum foil. The actuation strain was determined optically with a digital camera detecting the edge between the black electrode and the light silicone film, thus measuring the extension of the electrode diameter. The extension was measured at two different positions and the values were averaged. The stack actuators were tested with the same voltage source as the single-layer actuators at frequencies between 0.1 to 100 Hz and Voltages between 0 to 5.6 kV. The change in the thickness of the stack was followed by a laser measuring the distance from the laser to the top of the stack.

NMR Spectroscopy: ^1H and ^{13}C NMR spectra were recorded at 298 K on a Bruker Avance 400 NMR spectrometer using a 5 mm broadband inverse probe at 400.13 and 100.61 MHz, respectively. Chemical shifts (δ) in ppm are calibrated to residual solvent peaks ($CDCl_3$: δ = 7.26 and 77.16 ppm)

Gel Permeation Chromatography: Gel permeation chromatograms (GPC) were recorded using an Agilent 1100 Series HPLC (columns: serial coupled PSS SDV 5 m, 100 Å and PSS SDV 5 m, 1000 Å, detector: DAD, 235 and 360 nm; refractive index), where THF was the mobile phase. Poly(methyl methacrylate) (PMMA) was used as standard.

Differential Scanning Calorimetry: Differential scanning calorimetry (DSC) investigations were undertaken on a PerkinElmer Pyris Diamond instrument under a nitrogen flow (50 mL min^{-1}) in aluminum crucibles, which were shut with pierced lids and contained ≈10 mg sample mass. Two heating and one cooling steps with a heating and cooling rate of 20 K min^{-1} were conducted per measurement under a nitrogen flow (50 mL min^{-1}). The second heating step was considered for the evaluation of the T_g.

Thermalgravimetric Analysis: Thermalgravimetric Analysis (TGA) was performed with a *Netzsch* TG 209-F1 with vacuum-tight thermomicrobalance. Samples were measured in an Al_2O_3 crucible at a heating rate of 20 K min^{-1} under air flow.

Scanning Electron Microscopy: Scanning electron microscopy (SEM) images were recorded on a FEI Quanta 650 ESEM. Images were taken in secondary electrons-topography mode using Everhart–Thornley Detector at 20 kV acceleration voltage.

Supporting Information

Supporting Information is available from the Wiley Online Library or from the author.

Acknowledgements

The authors gratefully acknowledge the financial support from the Swiss Federal Laboratories for Materials Science and Technology (Empa), the project MANUFHAPTICS of the Strategic Focus Area (SFA) Advanced Manufacturing of the ETH Board, and the European Research Council (ERC) under the European Union's Horizon 2020 research and innovation programme (grant agreement No. 101001182). The authors also acknowledge Dr. G. Kovacs (Empa) for providing access to the electromechanical test equipment, Dr. M. Barbezat (Empa) for providing access to the rheometer, Ms. T. Künniger for her support with the DMA measurements, L. Düring (CT Systems) for his continuous support with technical issues, D. Rentsch (Empa) for his support with the NMR measurements, and H. Shea (EPFL) for stimulating discussions.

Conflict of Interest

P.M.D., T.P., A.V.B., J.V. & D.M.O. have a patent application comprising the capillary suspension of polar and non-polar polysiloxanes. The remaining authors declare no competing financial interests.

Data Availability Statement

The data that support the findings of this study are openly available in Zenodo at https://doi.org/10.5281/zenodo.8355222, reference number 8355222.

Keywords

3D printing, capillary suspensions, dielectric elastomer actuators (DEA), high-permittivity elastomers, multimaterial printing

Received: November 21, 2023
Revised: December 11, 2023
Published online:

[1] S. Roh, L. B. Okello, N. Golbasi, J. P. Hankwitz, J. A.-C. Liu, J. B. Tracy, O. D. Velev, *Adv. Mater. Technol.* **2019**, *4*, 1800528.
[2] M. Wehner, R. L. Truby, D. J. Fitzgerald, B. Mosadegh, G. M. Whitesides, J. A. Lewis, R. J. Wood, *Nature* **2016**, *536*, 451.
[3] M. Schaffner, J. A. Faber, L. Pianegonda, P. A. Rühs, F. Coulter, A. R. Studart, *Nat. Commun.* **2018**, *9*, 878.
[4] A. V. Bayles, T. Pleij, M. Hofmann, F. Hauf, T. Tervoort, J. Vermant, *ACS Appl. Mater. Interfaces* **2022**, *14*, 15667.
[5] L. A. E. Müller, A. Demongeot, J. Vaucher, Y. Leterrier, J. Avaro, M. Liebi, A. Neels, I. Burgert, T. Zimmermann, G. Nyström, G. Siqueira, *ACS Appl. Mater. Interfaces* **2022**, *14*, 16703.
[6] E. Sachyani Keneth, A. Kamyshny, M. Totaro, L. Beccai, S. Magdassi, *Adv. Mater.* **2021**, *33*, 2003387.
[7] M. A. S. R. Saadi, A. Maguire, N. T. Pottackal, M.d S. H. Thakur, M. M.d. Ikram, A. J. Hart, P. M. Ajayan, M. M. Rahman, *Adv. Mater.* **2022**, *34*, 2108855.
[8] S. Schlatter, G. Grasso, S. Rosset, H. Shea, *Adv. Intell. Syst.* **2020**, *2*, 2000136.
[9] A. Chortos, E. Hajiesmaili, J. Morales, D. R. Clarke, J. A. Lewis, *Adv. Funct. Mater.* **2020**, *30*, 1907375.
[10] A. Chortos, J. Mao, J. Mueller, E. Hajiesmaili, J. A. Lewis, D. R. Clarke, *Adv. Funct. Mater.* **2021**, *31*, 2010643.
[11] N. M. Larson, J. Mueller, A. Chortos, Z. S. Davidson, D. R. Clarke, J. A. Lewis, *Nature* **2023**, *613*, 682.
[12] G. Gallone, F. Galantini, F. Carpi, *Polym. Int.* **2010**, *59*, 400.
[13] J. E. Q. Quinsaat, M. Alexandru, F. A. Nüesch, A. Borgschulte, D. M. Opris, *J. Mater. Chem. A* **2012**, 14.
[14] M. Molberg, D. Crespy, P. Rupper, F. Nüesch, J.-A. E. Månson, C. Löwe, D. M. Opris, *Adv. Funct. Mater.* **2010**, *20*, 3280.
[15] X. Liu, L. Yu, Y. Nie, A. L. Skov, *Adv. Eng. Mater.* **2019**, *21*, 1900481.
[16] S. J. Dünki, Y. S. Ko, F. A. Nüesch, D. M. Opris, *Adv. Funct. Mater.* **2015**, *25*, 2467.
[17] Y. Sheima, Y. Yuts, H. Frauenrath, D. M. Opris, *Macromolecules* **2021**, *54*, 5737.
[18] Y. Sheima, J. Von Szczepanski, P. M. Danner, T. Künniger, A. Remhof, H. Frauenrath, D. M. Opris, *ACS Appl. Mater. Interfaces* **2022**, *14*, 40257.
[19] D. M. Opris, *Adv. Mater.* **2018**, *30*, 1703678.
[20] Y. Sheima, P. Caspari, D. M. Opris, *Macromol. Rapid Commun.* **2019**, *40*, 1900205.
[21] J. Von Szczepanski, P. M. Danner, D. M. Opris, *Adv. Sci.* **2022**, *9*, 2202153.
[22] E. Perju, S. Shova, D. M. Opris, *ACS Appl. Mater. Interfaces* **2020**, *12*, 23432.
[23] G. Kovacs, L. Düring, S. Michel, G. Terrasi, *Sens. Actuators Phys.* **2009**, *155*, 299.
[24] Z. Li, M. Sheng, M. Wang, P. Dong, B. Li, H. Chen, *Smart Mater. Struct.* **2018**, *27*, 075023.
[25] F. B. Madsen, A. E. Daugaard, S. Hvilsted, A. L. Skov, *Macromol. Rapid Commun.* **2016**, *37*, 378.
[26] J. Von Szczepanski, D. M. Opris, *Adv. Mater. Technol.* **2023**, *8*, 2201372.
[27] G. Siqueira, D. Kokkinis, R. Libanori, M. K. Hausmann, A. S. Gladman, A. Neels, P. Tingaut, T. Zimmermann, J. A. Lewis, A. R. Studart, *Adv. Funct. Mater.* **2017**, *27*, 1604619.
[28] J. A. Lewis, *Adv. Funct. Mater.* **2006**, *16*, 2193.
[29] C. Perrinet, E.-J. Courtial, A. Colly, C. Marquette, R. Fulchiron, *Adv. Mater. Technol.* **2020**, *5*, 1901080.
[30] T. J. Hinton, A. Hudson, K. Pusch, A. Lee, A. W. Feinberg, *ACS Biomater. Sci. Eng.* **2016**, *2*, 1781.
[31] Y. Wang, N. Willenbacher, *Adv. Mater.* **2022**, *34*, 2109240.
[32] S. Roh, D. P. Parekh, B. Bharti, S. D. Stoyanov, O. D. Velev, *Adv. Mater.* **2017**, *29*, 1701554.
[33] M. J. Ford, C. K. Loeb, L. X. P. Pérez, S. Gammon, S. Guzorek, H. B. Gemeda, A. M. Golobic, A. Honnell, J. Erspamer, E. B. Duoss, T. S. Wilson, J. M. Lenhardt, *Adv. Mater. Technol.* **2022**, *7*, 2100974.
[34] J. Suriboot, A. C. Marmo, B. K. D. Ngo, A. Nigam, D. Ortiz-Acosta, B. L. Tai, M. A. Grunlan, *Soft Matter* **2021**, *17*, 4133.
[35] J. Beach, S. Mann, C. Ault, D. Radojcic, X. Wan, A. Zlatanic, S. Patterson, J. M. Messman, P. R. Dvornic, *Macromolecules* **2021**, *54*, 1715.
[36] E. Koos, N. Willenbacher, *Science* **2011**, *331*, 897.
[37] J. Dittmann, J. Maurath, B. Bitsch, N. Willenbacher, *Adv. Mater.* **2016**, *28*, 1689.
[38] H. Ding, S. Barg, B. Derby, *Nanoscale* **2020**, *12*, 11440.
[39] D. Menne, L. Lemos Da Silva, M. Rotan, J. Glaum, M. Hinterstein, N. Willenbacher, *ACS Appl. Mater. Interfaces* **2022**, *14*, 3027.
[40] M. Schneider, E. Koos, N. Willenbacher, *Sci. Rep.* **2016**, *6*, 31367.
[41] P. Mazurek, S. Vudayagiri, A. L. Skov, *Chem. Soc. Rev.* **2019**, *48*, 1448.
[42] E. Koos, N. Willenbacher, *Soft Matter* **2012**, *8*, 3988.
[43] H. Sun, Z. Han, N. Willenbacher, *ACS Appl. Mater. Interfaces* **2019**, *11*, 38092.
[44] S. Abdolhosseinzadeh, C. Zhang, R. Schneider, M. Shakoorioskooie, F. Nüesch, J. Heier, *Adv. Mater.* **2022**, *34*, 2103660.
[45] P. M. Danner, M. Iacob, G. Sasso, I. Burda, B. Rieger, F. Nüesch, D. M. Opris, *Macromol. Rapid Commun.* **2022**, 2100823.
[46] S. Bindgen, J. Allard, E. Koos, *Curr. Opin. Colloid Interface Sci.* **2022**, *58*, 101557.
[47] S. Roh, L. B. Okello, N. Golbasi, J. P. Hankwitz, J. B. Tracy, O. D. Velev, **2019**, *6*.
[48] Y. Yu, B. Huang, Y. Zhao, Y. Zhao, L. Dai, Z. Zhang, H.-F. Fei, *ACS Appl. Polym. Mater.* **2023**, *5*, 259.
[49] F. B. Albuquerque, H. Shea, *Smart Mater. Struct.* **2021**, *30*, 125022.
[50] M. Hu, C.-P. Hsu, L. Isa, *Langmuir* **2020**, *36*, 11171.
[51] M. Mooney, *J. Rheol.* **1931**, *2*, 210.
[52] J. Mewis, N. J. Wagner, *Colloidal Suspension Rheology*, Cambridge University Press, Cambridge, **2011**.